

AN ABSTRACT OF THE THESIS OF

Karlan Stephen Wolfkill for the degree of Master of Science in Mathematics presented
on June 13, 2012.

Title: Pseudo-spectral Approximations of Rossby and Gravity Waves in a Two-layer Fluid

Abstract approved: _____

Robert L. Higdon

The complexity of numerical ocean circulation models requires careful checking with a variety of test problems. The purpose of this paper is to develop a test problem involving Rossby and gravity waves in a two-layer fluid in a channel. The goal is to compute very accurate solutions to this test problem. These solutions can then be used as a part of the checking process for numerical ocean circulation models.

Here, Chebychev pseudo-spectral methods are used to solve the governing equations with a high degree of accuracy. Chebychev pseudo-spectral methods can be described in the following way: For a given function, find the polynomial interpolant at a particular non-uniform grid. The derivative of this polynomial serves as an approximation to the derivative of the original function. This approximation can then be inserted to differential equations to solve for approximate solutions. Here, the governing equations reduce to an eigenvalue problem with eigenvectors and eigenvalues corresponding to the spatial dependences of modal solutions and the frequencies of those solutions, respectively.

The results of this method are checked in two ways. First, the solutions using the Chebychev pseudo-spectral methods are analyzed and are found to exhibit the properties known to belong to physical Rossby and gravity waves. Second, in the special case

where the two-layer model degenerates to a one-layer system, some analytic solutions are known. When the numerical solutions are compared to the analytic solutions, they show an exponential rate of convergence.

The conclusion is that the solutions computed using the Chebychev pseudo-spectral methods are highly accurate and could be used as a test problem to partially check numerical ocean circulation models.

©Copyright by Karlan Stephen Wolfkill

June 13, 2012

All Rights Reserved

Pseudo-spectral Approximations of Rossby and Gravity Waves in a Two-layer Fluid

by

Karlan Stephen Wolfkill

A THESIS

submitted to

Oregon State University

in partial fulfillment of
the requirements for the
degree of

Master of Science

Presented June 13, 2012
Commencement June 2012

Master of Science thesis of Karlan Stephen Wolfkill presented on June 13, 2012

APPROVED:

Major Professor, representing Mathematics

Chair of the Department of Mathematics

Dean of the Graduate School

I understand that my thesis will become part of the permanent collection of Oregon State University libraries. My signature below authorizes release of my thesis to any reader upon request.

Karlan Stephen Wolfkill, Author

ACKNOWLEDGEMENTS

Academic

I am indebted to my advisor, Dr. Robert Higdon, for suggesting the topic and for the continued support throughout the research and writing process. I also wish to acknowledge Bethany Pratt for help with the editing of this paper.

Personal

I'm especially grateful to Glenn and Jeenie Balkins for the constant encouragement and for opening their home to me. I'm also grateful to Bruce and Bethany Pratt for listening and understanding throughout the process of writing this paper. I also wish to thank my family, and my fiancée, Leonor Santos, for all the prayers and moral support.

TABLE OF CONTENTS

	<u>Page</u>
1. INTRODUCTION	1
2. GOVERNING EQUATIONS	3
3. FORMULATING THE PROBLEM	7
3.1. Set-up	7
3.2. An eigenvalue problem	7
4. A NUMERICAL METHOD	9
4.1. Chebychev interpolation	10
4.2. Chebychev differentiation	13
4.3. Application to the ocean eigenvalue problem	14
5. DISCRETIZATION OF THE EIGENVALUE PROBLEM	15
5.1. Boundary conditions	17
5.2. Eigenvalues and eigenvectors	18
6. RESULTS	19
6.1. Existence of Rossby modes using this scheme	19
6.2. Dispersion relation for Rossby waves	21
6.3. Contour plots and velocity fields	22
6.4. Kelvin modes	24
7. EXACT SOLUTIONS FOR A SPECIAL CASE	26
7.1. Convergence of Chebychev solution to analytic solution	32

TABLE OF CONTENTS (Continued)

	<u>Page</u>
8. CONCLUSION	33
BIBLIOGRAPHY	36

LIST OF FIGURES

Figure	Page
<p>4.1 Interpolating the function $f(x) = 1/(1+9x^2)$ on the interval $[-1, 1]$ using a uniform grid of 15 points. The oscillatory behavior of the interpolating polynomial near the boundary using the uniform grid introduces error that increases and the degree of polynomial increases. It is clear that the derivative of this polynomial will also have this error, thus it will not be a good approximation to f'.</p>	11
<p>4.2 Interpolating the function $f(x) = 1/(1+9x^2)$ on the interval $[-1, 1]$ using a Chebychev grid of 15 points. Using the nonuniform grid, the oscillations near the boundary are minimized. Graphically, it is seen that not only is the interpolating polynomial a close approximation to f, the derivative of the interpolating polynomial is approximately equal to f'</p>	12
<p>6.1 Eigenvalues with variable Coriolis parameter. Here the Coriolis parameter is given by $f(y) = f_0 + \beta y$ where f_0 is the Coriolis parameter at 45° N, the center of the channel. The eigenvalues are ordered according to absolute value and the mode number just refers to this ordering. The number of interpolation points in this case is $N = 32$, so there are $6 * N - 4 = 188$ modes. Modes from 1-60 are Rossby modes with external and internal modes generally alternating. Closer to 60 are the well-resolved modes. Modes 61-123 are internal gravity modes. Of these, modes 61-64 are the internal Kelvin modes, immediately followed by the internal Poincaré modes. Modes 124-188 are external gravity modes. Modes 124-127 are Kelvin modes and are immediately followed by the external Poincaré modes.</p>	20
<p>6.2 Eigenvalues with fixed Coriolis parameter. Here the Coriolis parameter is given by $f = f_0$ where f_0 is the Coriolis parameter at the 45° N, the center of the channel. Here modes 61-188 appear as they did in Figure 6.1, but modes 1-60 do not appear. They are not shown because they are very near machine epsilon. This demonstrates that these modes only exist because of the dependence of f on y in the β-plane problem.</p>	21
<p>6.3 Dispersion relations for some numerical Rossby modes. Here $\Delta x = 10$ km. Observe that for all values of k, the phase velocity w/k is negative (westward). However, while for small values of k (long wavelengths) the group velocity $d\omega/dk$ is negative (westward), the group velocity for larger values of k (short waves) is have positive (eastward).</p>	22

LIST OF FIGURES (Continued)

<u>Figure</u>	<u>Page</u>
<p>6.4 First external Rossby mode. This shows the perturbation of the layer thickness for layers 1 and 2 as well as the perturbation in the free-surface elevation. Solid curves correspond to positive perturbation and dotted lines to negative perturbation. This mode corresponds to mode number 60 in Figure 6.1 and is the first external Rossby mode in the sense that it is the external Rossby mode that varies least in the cross-channel direction. In each subplot the intervals between contours are the same. Since there are three times more contours in the plot of layer 2, the perturbation in the thickness of layer 2 is three times greater than the perturbation in the thickness of layer 1. This is consistent since layer 2 is three times thicker than layer 1 at equilibrium. Notice that the layers thicken or thin together, so that the effect on the free-surface elevation is the sum of the perturbations in each layer. Thus there are four times as many contours in the plot showing perturbation in free-surface elevation as there are in the plot showing perturbation in the thickness of layer 1.</p>	23
<p>6.5 Velocity fields for the first external Rossby mode. These are the velocity fields corresponding to the mode shown in Figure 6.4. Observe that the velocity field arrows are approximately tangent to the level curves shown in Figure 6.4 with clockwise circulation corresponding to crests and counterclockwise circulation corresponding to troughs. Also, at any point the circulation is in the same direction in both layers. This is characteristic of external Rossby modes.</p>	24
<p>6.6 First internal Rossby mode. This mode corresponds to the mode number 58 from Figure 6.1. Again, “first” refers to the fact that this is the internal Rossby mode with the least variation in the cross-channel direction. Here the number of contours is the same in both layers but where layer 1 has a positive perturbation, layer 2 has a negative perturbation and vice versa. Thus the net effect on the free-surface perturbation is nearly zero. Thus the plot showing free-surface elevation is blank.</p>	25
<p>6.7 Velocity fields for the first internal Rossby mode. These are the velocity fields corresponding to layer 1 and layer 2 in the mode shown in Figure 6.6. Observe that the layers show circulation along the level curves as in the external mode, but that layers circulate in opposite directions. In fact, the mass-weighted average of the velocities in the two layers is nearly zero. In the thinner layer, layer 1, the magnitude of the velocity is 3 times that of layer 2. While it is true, this is difficult to see using this type of plot.</p>	26

LIST OF FIGURES (Continued)

<u>Figure</u>	<u>Page</u>
6.8 Second external Rossby mode. This mode corresponds to mode number 59 in Figure 6.1.	27
6.9 Velocity fields for the second external Rossby mode. These velocity fields correspond to the mode shown in Figure 6.8.	28
6.10 Second internal Rossby mode. This mode corresponds to the mode number 57 in Figure 6.1.	29
6.11 Velocity fields for the second internal Rossby mode. These velocity fields correspond to the mode shown in Figure 6.10.	30
6.12 A Kelvin mode. This is the cross-channel profile of the internal Kelvin wave that travels along the South edge of the channel. The first column of figures corresponds to the upper layer, and the second column corresponds to the lower layer. Note that, consistent with the theory, there is exponential decay in Δp_r from one side of the domain. Furthermore, the phase velocity of this wave is found to be positive, thus this wave is travelling eastward. This is also consistent with the theory that states that Kelvin waves propagate in a counterclockwise fashion in the northern hemisphere.	31
7.1 Normalized cross-channel velocity, exact and approximate, for the first Poincaré mode. V is an imaginary constant multiple of the cross-channel velocity. This plot shows the cross-channel profile of V for $x = 0$. Here both solutions are normalized to have maximum value 1.	33
7.2 The rate of convergence of the max-norm error. The error here is taken to be the maximum difference between the approximated solution and the exact solution at interpolation points. The vertical axis shows the base 10 logarithm of this error. There is a slight difference in error between the even and odd number of interpolation points. Still, the relation between the number of interpolation points and the logarithm of the max-error is nearly linear. Thus, the error decreases exponentially as the number of interpolation points increase. This is consistent with the order of convergence given in Theorem 4.1.1.	34
7.3 Normalized cross-channel velocity of the approximate and exact solutions for the second Poincaré mode.	35
7.4 The rate of convergence of the max-norm error. A few more interpolation points are needed to reach the minimum error, but the rate of convergence is still clearly exponential. At about 20 interpolation points the pseudo-spectral method produces a nearly exact solution.	36

PSEUDO-SPECTRAL APPROXIMATIONS OF ROSSBY AND GRAVITY WAVES IN A TWO-LAYER FLUID

1. INTRODUCTION

The purpose of this paper is to develop highly accurate solutions of a test problem involving Rossby and gravity waves with the intention that these solutions could be used for partial testing of numerical models of ocean circulation. Specifically, the problem is: Given a hydrostatic fluid with two layers of constant density in a channel running East-West, find nearly analytic representations of the internal and external Rossby and gravity waves that occur in the channel. Some manipulation of the governing equations leads to a differential-algebraic eigenvalue problem. To solve this, Chebychev pseudo-spectral differentiation is employed in hopes of achieving spectral accuracy. The solutions are then compared with the theory and, in a special case, with known analytic formulas. These comparisons provide evidence that this method does produce highly accurate representations of the solution to the test problem.

Section 2. introduces the governing equations, as presented by Higdon [2]. These governing equations can be thought of as two linearized systems of partial differential equations similar to the Linearized Shallow-Water Equations, each corresponding to one layer in the fluid. The two systems are coupled. Together with an interface jump condition, these systems comprise the governing equations.

These governing equations rely on the assumption that the vertical scale is much smaller than the horizontal scale of the waves being modeled, so the fluid is nearly hydrostatic. Also, they are linearized, so they require the assumption that the general state

is a small perturbation from a static state. Thus, nonlinear factors are negligible. The dependent variables are horizontal velocity in each layer and the perturbations in the differences in pressure from the bottom to the top of each layer, which can be thought of as “perturbation in layer thicknesses.” The independent variables are horizontal coordinates and time.

Section 3. formally develops the channel problem as an eigenvalue problem with boundary conditions due to the hard wall of the channel on the North and South edges. It is assumed that the solutions, which consist of the horizontal velocity and perturbation in pressure difference for each layer, are continuous in time and in the East-West (x) direction. It is possible to take the Fourier transform of the system to eliminate derivatives with respect to these variables. The resulting system is a differential-algebraic eigenvalue problem, that is, an eigenvalue problem involving equations that are purely algebraic as well as equations involving derivatives with respect to the North-South (y) variable. In the following sections, this eigenvalue problem will be numerically solved using Chebychev pseudo-spectral methods, by discretizing on a non-uniform grid in y and replacing the derivatives with Chebychev differentiation matrices.

Section 4. introduces Chebychev interpolation and pseudo-spectral differentiation. To approximate the derivative of a function, first interpolate the function using a polynomial and then differentiate that polynomial and use the result to estimate the derivative of the original function. Using a uniform grid for polynomial interpolation can lead to large error due to oscillation near the endpoints. To avoid this, interpolate the function using a non-uniform grid called a Chebychev grid. In a Chebychev grid the interpolation points are clustered near the endpoints to prevent spurious oscillations.

Section 5. describes the discretization of the differential-algebraic eigenvalue problem using Chebychev differentiation and reduces the problem to a purely algebraic eigenvalue problem that can be solved using MATLAB. Up to an imaginary multiple, the eigenvalues

are wave frequencies, and their corresponding eigenvectors give the spatial dependence of solutions in the cross-channel direction.

In Section 6. some numerical Rossby and Kelvin modes are shown and discussed. These numerical solutions are qualitatively consistent with the theory. First, by comparing the case where the Coriolis parameter f varies with y to the case where f is held constant, it is demonstrated that this method does produce Rossby modes. Then, the dispersion relations for some of these Rossby modes are shown and are consistent with the theory. Next, this section includes plots of the first and second internal and external Rossby modes, where “first” refers to the wave with least cross-channel variation, and the second mode varies second least. Next, the numerical Kelvin modes are discussed, including a plot of the cross-channel profile of an internal Kelvin mode. It is shown that these Kelvin modes propagate in a counterclockwise fashion, again, consistent with the theory.

Section 7. considers a special case in which exact solutions are known. When the densities of the two layers are equal, this system degenerates to the Linearized Shallow-Water equations. In the case where f is held constant across the channel, the exact solution for Poincaré modes is known. In this special case the Chebychev pseudo-spectral approximations converge exponentially to the exact solutions, consistent with the theory of pseudo-spectral methods.

2. GOVERNING EQUATIONS

Consider a fluid with two layers of constant density. Assume that for each layer the thickness of the fluid is much smaller than the horizontal scale. This is the same assumption used to construct the related Shallow-Water Equations. This assumption

implies that any vertical acceleration is negligible, thus the fluid is nearly hydrostatic. Next, assume that the flow is a small perturbation of a static state in which the surface of the water, the layer interface, and the bottom are all level. Thus, any non-linear factors are negligible. This leads to the linearized governing equations as presented in [2].

Let $r = 1$ indicate the top layer and let $r = 2$ indicate the bottom layer. Also, when referring to a layer interface, let $r = 2$ indicate the bottom of layer 2, and let $r = 1$ indicate the bottom of layer 1 and let $r = 0$ the free surface. So, for $r = 1, 2$ let u_r and v_r be the velocity in the x (East-West) and y (North-South) directions, respectively, in layer r .

Given the static state, let \tilde{p}_r be the equilibrium pressure at the bottom of layer r . Given a small perturbation from the static state, let the pressure at the bottom of layer r be $\tilde{p}_r + p_r$. Thus, the difference in pressure from the bottom of a layer to the top of a layer is $(\tilde{p}_r - \tilde{p}_{r-1}) + (p_r - p_{r-1}) = \Delta\tilde{p}_r + \Delta p_r$. Hence, define $\Delta\tilde{p}_r$ to be the equilibrium difference in pressure from the bottom to the top of a layer and Δp_r to be the perturbation in that difference.

Now, since the fluid is hydrostatic, the vertical pressure difference over layer r is the weight per unit horizontal area in layer r . Because of the assumption of constant density in each layer, the thickness of layer r can be directly determined by the relation $(\Delta\tilde{p}_r + \Delta p_r) = \rho_r g (\Delta\tilde{z}_r + \Delta z_r)$ where $\Delta\tilde{z}_r$ is the equilibrium thickness of layer r and Δz_r is the perturbation of layer thickness, ρ_r is the density of layer r , and g is acceleration due to gravity. Thus, $\Delta\tilde{p}_r$ and Δp_r can be informally thought of as the equilibrium thickness of layer r and the perturbation of thickness of layer r respectively.

Furthermore, let $M = \alpha p + gz$ be the Montgomery potential at any given elevation z where $\alpha = 1/\rho$ is specific volume. Let α_r denote the specific volume of layer r . For a hydrostatic fluid of constant density, the Montgomery potential is independent of depth. So, let \tilde{z}_r be the elevation of the bottom of layer r . For each layer r , the Montgomery

potential at equilibrium can be written $\tilde{M}_r = \alpha_r \tilde{p}_r + g \tilde{z}_r$, and the Montgomery potential for a small perturbation from equilibrium can be written $\tilde{M}_r + M_r = \alpha_r (\tilde{p}_r + p_r) + g (\tilde{z}_r + z_r)$. Thus, the perturbation in Montgomery potential can be written $M_r = \alpha_r p_r + g z_r$. Finally, let f be the Coriolis parameter, which depends on y .

Then, the governing equations are

$$\begin{aligned} \frac{\partial u_r}{\partial t} - f v_r &= -\frac{\partial M_r}{\partial x} \\ \frac{\partial v_r}{\partial t} + f u_r &= -\frac{\partial M_r}{\partial y} \\ \frac{\partial}{\partial t}(\Delta p_r) + \Delta \tilde{p}_r \left(\frac{\partial u_r}{\partial x} + \frac{\partial v_r}{\partial y} \right) &= 0, \end{aligned} \tag{2.1}$$

together with the jump condition $M_1 - M_2 = p_1(\alpha_1 - \alpha_2)$.

Given appropriate initial and boundary conditions, several types of waves are solutions of this system [3]. The first type is a gravity wave. In gravity waves, a perturbation in layer thickness is counteracted by gravity resulting in harmonic oscillations. Gravity waves occur in two forms. In an open domain these are approximately sinusoidal in x and y and are called Poincaré waves. In a bounded domain a second type of gravity wave occurs called a Kelvin wave. Kelvin waves only form in a rotating reference frame. The profile of a Kelvin wave is of exponential decay from one side of the domain. In the northern hemisphere Kelvin waves always propagate in a counter-clockwise fashion. That is, a Kelvin wave that appears on the North edge of a domain will travel westward, while a Kelvin wave on the South edge of a domain will travel eastward.

Besides gravity waves, another type of wave solution of (2.1) is a Rossby wave. Rossby waves result from the dependence of the Coriolis parameter f on y and on variation in bottom topography. Instead of gravity, the restoring mechanism in these waves is vorticity, and they can be derived from the conservation of potential vorticity [3]. The conservation of potential vorticity can be stated

$$\frac{D}{Dt} \left(\frac{f + \xi}{h} \right) = 0.$$

Here, f is the Coriolis parameter, $\xi = v_x - v_y$ is vorticity (in the z direction) and h is the fluid thickness. The operator $\frac{D}{Dt}$ is the material derivative, the derivative with respect to time in a reference frame that moves with the fluid. This shows there are two ways to generate Rossby waves. The first way is by changing h . These Rossby waves are called topographical Rossby waves because they depend on bottom topography. Since the current test problem concerns a channel with a fixed flat bottom, these will not be considered here.

The second way to generate Rossby waves is to change f . These are called planetary Rossby waves because they depend on the planetary parameter f . For example, consider a column of water in the northern hemisphere. If this column moves northward its Coriolis parameter increases, causing the relative vorticity to decrease and resulting in clockwise rotation. This, in turn, causes nearby water to rotate and a wave, propagating East to West, is generated. Long Rossby waves are nearly non-dispersive and are known to cross entire ocean basins. Rossby waves are believed to play an essential role in ocean circulation, so it is important the model incorporates these waves. An interesting characteristic of Rossby waves is that they are in near geostrophic balance [3]. That is, the velocity field of the fluid in a Rossby wave is normal to the pressure gradient. (See Section 6.3.)

In a two-layer system these waves occur in two different forms. The first is as external modes, where the layer thickness perturbation of each layer changes together in the same direction. That is, the two layers thicken or thin together, and the relative perturbations in the layer thicknesses are approximately equal. So, the profile of the free surface and the profile of the layer interface have the same shape. The second class of waves in the two-layer system consists of internal waves. These waves travel along the layer interface and the layer thickness in each layer changes oppositely so that the total perturbation of the free surface at the top of the fluid is nearly zero.

3. FORMULATING THE PROBLEM

3.1. Set-up

Consider a channel with nearly the same parameters as found in [2]. Let the channel be 320km wide and be oriented East-West. So, $-\infty < x < \infty$ and $-160000 < y < 160000$ where $y = -160000$ is the South edge of the channel and $y = 0$ is the center of the channel. Let the equilibrium thickness of the top layer be $\Delta\tilde{p}_1 = 1000\text{m}$ and of the bottom layer be $\Delta\tilde{p}_2 = 3000\text{m}$. Let the specific volumes be $\alpha_1 = 0.975 \times 10^{-3}$ and $\alpha_2 = 0.972 \times 10^{-3}$.

Now, for the Coriolis parameter f , use a β -plane approximation $f(y) = f_o + \beta y$ where f_o is the Coriolis parameter at the center of the channel. In this case take the center of the channel to be 45° N. So, $f_o = 2R \sin(45^\circ)$, where $R = 6378100\text{m}$, the approximate radius of the Earth, and $\beta = 2R \cos(45^\circ)/\Omega$ where $\Omega = 2\pi/86400$ radians/s is the approximate rate of rotation of the Earth.

3.2. An eigenvalue problem

To transform (2.1) into a solvable problem, first consider the perturbation Montgomery potential for layer r , defined in Section 2. to be $M_r = \alpha_r p_r + g z_r$. For the case where $r = 2$, the perturbation of the bottom of layer 2, z_2 , is always zero. (This is the channel floor.) Also, $p_2 = \Delta p_1 + \Delta p_2$, the combined perturbation in pressure above the channel floor. Thus, $M_2 = \alpha_2(\Delta p_1 + \Delta p_2)$. Then, using the jump condition $M_1 - M_2 = p_1(\alpha_1 - \alpha_2)$, together with the fact that p_1 , the perturbation in the pressure at the bottom of layer 1, is equal to Δp_1 (assume constant pressure at the top of the water), $M_1 = M_2 + p_1(\alpha_1 - \alpha_2) = \alpha_1 \Delta p_1 + \alpha_2 \Delta p_2$. Hence, it is now possible to eliminate the

Montgomery potential using the substitution

$$M_r = \alpha_r \Delta p_1 + \alpha_2 \Delta p_2.$$

The system becomes

$$\begin{aligned} \frac{\partial u_r}{\partial t} - f v_r &= -\alpha_r \frac{\partial}{\partial x}(\Delta p_1) - \alpha_2 \frac{\partial}{\partial x}(\Delta p_2) \\ \frac{\partial v_r}{\partial t} + f u_r &= -\alpha_r \frac{\partial}{\partial y}(\Delta p_1) - \alpha_2 \frac{\partial}{\partial y}(\Delta p_2) \\ \frac{\partial}{\partial t}(\Delta p_r) + \Delta \tilde{p}_r \left(\frac{\partial u_r}{\partial x} + \frac{\partial v_r}{\partial y} \right) &= 0. \end{aligned} \quad (3.1)$$

Furthermore, assume the solution is continuous in x and t and take the Fourier transform of the system in these two variables. By canceling the common factors in each term and getting rid of the integrals it can be shown that this is equivalent to the substitution

$$\begin{aligned} u_r(x, y, t) &= \hat{u}_r(k, y, \omega) e^{ikx - i\omega t} \\ v_r(x, y, t) &= \hat{v}_r(k, y, \omega) e^{ikx - i\omega t} \\ \Delta p_r(x, y, t) &= \Delta \hat{p}_r(k, y, \omega) e^{ikx - i\omega t} \end{aligned} \quad (3.2)$$

Observe that derivatives in x and t become multiplications by ik and $-i\omega$ respectively. Thus, this substitution will eliminate any derivative with respect to the x and t variables. Unfortunately, it is not possible to take the Fourier transform in y , since f depends on y .

After the substitution, cancel the common factor of $e^{ikx - i\omega t}$. The system reduces to

$$\begin{aligned} (-i\omega) \hat{u}_r &= f \hat{v}_r - ik \alpha_r \Delta \hat{p}_1 - ik \alpha_2 \Delta \hat{p}_2 \\ (-i\omega) \hat{v}_r &= -f \hat{u}_r - \alpha_r \frac{\partial}{\partial y}(\Delta \hat{p}_1) - \alpha_2 \frac{\partial}{\partial y}(\Delta \hat{p}_2) \\ (-i\omega) \Delta \hat{p}_r &= -\Delta \tilde{p}_r (ik \hat{u}_r + \frac{\partial \hat{v}_r}{\partial y}). \end{aligned} \quad (3.3)$$

The channel wall requires that the y -velocity is zero at the channel wall, that is, for $r = 1, 2$,

$$v_r(k, y_S, \omega) = v_r(k, y_N, \omega) = 0$$

where $y_S = -160$ is the South wall of the channel and $y_N = 160$ is the North wall of the channel.

Now, (3.3) is a differential-algebraic eigenvalue problem. That is, it is an eigenvalue problem where differential equations are coupled with purely algebraic equations. The eigenfunctions of this system have six components,

$$(u_1(x, y, t), v_1(x, y, t), \Delta p_1(x, y, t), u_2(x, y, t), v_2(x, y, t), \Delta p_2(x, y, t)).$$

These eigenfunctions will be modal, physical solutions, and will include Poincaré, Kelvin and Rossby waves. The eigenvalues are wave frequencies.

Now, the goal is to solve the system (3.3) with solutions that are as accurate as possible. One way to do this is to approximate the solutions with polynomials. The challenge is to find the polynomials that achieve the desired accuracy. One method to do this is to use the polynomials described in Section 4. Since a polynomial of degree $N - 1$ is uniquely determined by its values at N points, (3.3) will reduce to a purely algebraic eigenvalue problem.

4. A NUMERICAL METHOD

This section describes the method of Chebychev differentiation. The strategy of Chebychev differentiation is to interpolate a function on a non-uniform grid and then to differentiate the interpolating polynomial and use this as an approximation to the derivative of the original function at the interpolation points. As will be seen in this section, this method can be highly accurate. Because both interpolation and polynomial differentiation are linear operations they can be represented as matrix multiplication. Thus, after a discretization of (3.3) in y , the differential operator $\frac{\partial}{\partial y}$ can be replaced with multiplication by D_N , the $N \times N$ Chebychev differentiation matrix. Do not confuse the notation of this section with the notation in the test problem. Here p_N will signify an

interpolating polynomial using N interpolation points, not a pressure.

4.1. Chebychev interpolation

With polynomial interpolation on a uniform grid, error can grow without bound due to oscillations as the degree of the polynomial increases. This is called Runge's phenomenon. Chebychev interpolation uses a non-uniform grid to minimize Runge's phenomenon, clustering the interpolation points near the edges of the domain to reduce spurious oscillations. This results in a high degree of accuracy and an exponential rate of convergence.

Figures 4.1 and 4.2 compare polynomial interpolation on a uniform grid to interpolation on a Chebychev grid, which is defined in equation (4.1). This is the famous Runge example. On the uniform grid large spurious oscillations occur near the boundary. However, using the Chebychev grid, the interpolating polynomial remains close to the exact solution.

In fact, we have the following theorem quoted by Trefethen [5] concerning the choice of interpolation points and the accuracy of the interpolating polynomial. This theorem borrows from electrostatic theory and uses the idea that the interpolation points are like point charges with a density function and potential.

Theorem 4.1..1 (Accuracy of polynomial interpolation) *Given a function g defined on $[-1, 1]$ and a sequence of sets of interpolation points $\{x_j\}_N$, $N = 1, 2, \dots$, that converge to a density function ρ on $[-1, 1]$ as $n \rightarrow \infty$ with corresponding potential ϕ given by*

$$\phi(z) = \int_{-1}^1 \rho(x) \log |z - x| dx,$$

define

$$\phi_{[-1,1]} = \sup_{x \in [-1,1]} \phi(x)$$

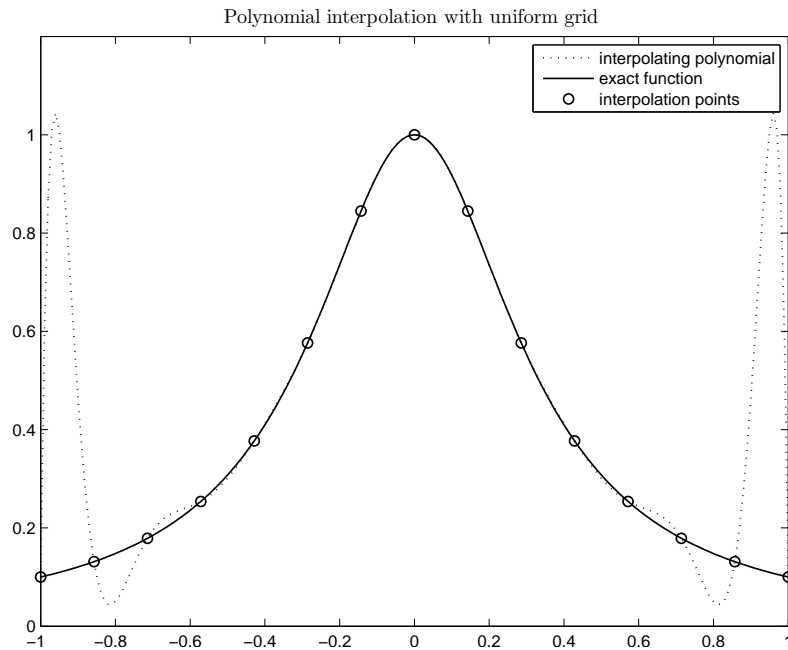


FIGURE 4.1: Interpolating the function $f(x) = 1/(1 + 9x^2)$ on the interval $[-1, 1]$ using a uniform grid of 15 points. The oscillatory behavior of the interpolating polynomial near the boundary using the uniform grid introduces error that increases and the degree of polynomial increases. It is clear that the derivative of this polynomial will also have this error, thus it will not be a good approximation to f' .

For each N construct the polynomial p_N of degree $\leq N - 1$ that interpolates g at the points $\{x_j\}_N$. If there exists a constant $\phi_g > \phi_{[-1,1]}$ such that g is analytic throughout the closed region

$$\{z \in \mathbb{C} : \phi(z) \leq \phi_g\},$$

then there exists a constant $C > 0$ such that for all $x \in [-1, 1]$ and all N ,

$$|g(x) - p_N(x)| \leq C e^{-N(\phi_g - \phi_{[-1,1]})}$$

The same estimate holds, though with a new constant C (still independent of x and N), for the difference of the ν th derivatives $g^{(\nu)} - p_N^{(\nu)}$, for any $\nu \geq 1$.

Now, if the hypotheses of this theorem hold, then not only will this method produce a interpolating polynomial whose error decreases exponentially as the number of interpolation points increases, but it will also produce a highly accurate polynomial approximation

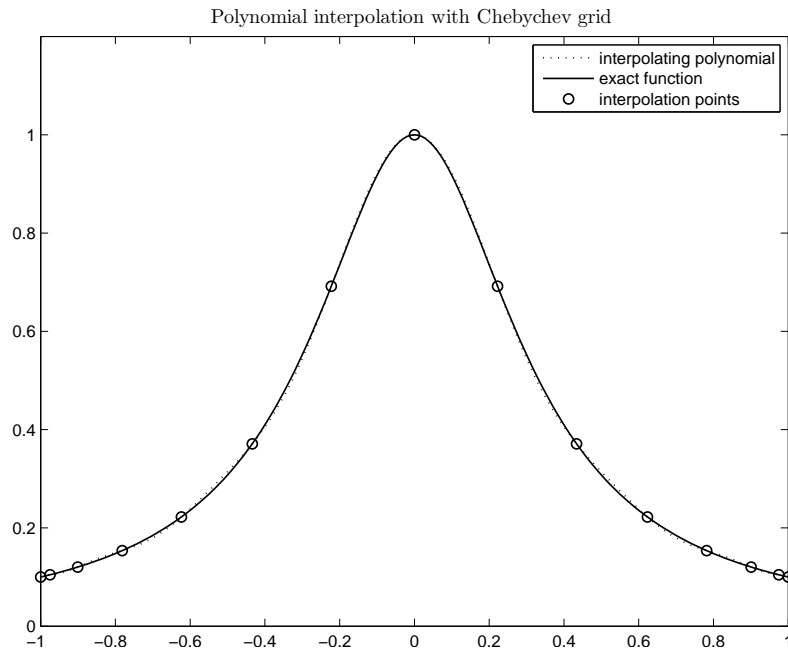


FIGURE 4.2: Interpolating the function $f(x) = 1/(1+9x^2)$ on the interval $[-1, 1]$ using a Chebychev grid of 15 points. Using the nonuniform grid, the oscillations near the boundary are minimized. Graphically, it is seen that not only is the interpolating polynomial a close approximation to f , the derivative of the interpolating polynomial is approximately equal to f'

to the *derivative* of a function. To show the hypotheses are satisfied, first, Trefethen [5] shows that the Chebychev interpolation points defined at

$$\xi_j = \cos(j\pi/N) \quad \text{for } j = 0, 1, 2, \dots, N \quad (4.1)$$

converge to the density function

$$\rho(x) = \frac{1}{\pi\sqrt{1-x^2}}, \quad x \in [-1, 1]. \quad (4.2)$$

So, the potential is

$$\phi(z) = \log \frac{|z - \sqrt{z^2 - 1}|}{2}. \quad (4.3)$$

As shown in [5], the level curves of this potential are ellipses with foci at -1 and 1 and the minimal level curve degenerates to the line segment $[-1, 1]$. So for $z = x \in [-1, 1]$, the potential reduces to the constant function $\phi(x) = -\log 2$. Thus, $\phi_{[-1,1]} = -\log 2$. Also

since the level curve $\phi(x) = -\log(2)$ is $[-1, 1]$ and *is a minimum*, the last part of the hypothesis requires that the function g to be interpolated be analytic on some complex region properly containing the interval $[-1, 1]$. If this holds, the rate of convergence is given by

$$|g(x) - p_N(x)| = \mathcal{O}(K^{-N}) \quad (4.4)$$

for K some positive constant greater than 1.

Now consider interpolating the solutions to the system (3.3). Let

$$q = (\hat{u}_1, \hat{v}_1, \Delta\hat{p}_1, \hat{u}_2, \hat{v}_2, \Delta\hat{p}_2)^T$$

be the solution to the system (3.3) with fixed k and ω . Let $q_{[-1,1]}$ be the solution scaled to the interval $[-1, 1]$ in y . It would be nice to show that $q_{[-1,1]}$ is analytic (in y) on some complex region properly containing $[-1, 1]$. For now, assume this condition is satisfied. A partial justification of this assumption is as follows: First, the solutions to the one-layer system do satisfy this hypothesis. They are linear combinations of parabolic cylinder functions, which are entire [4]. (See Section 7.) Secondly, the results of this paper rapidly converge to qualitatively accurate solutions. (See Section 6.)

4.2. Chebychev differentiation

According to Theorem 4.1..1, given a function g satisfying the hypothesis of the theorem, not only is the polynomial interpolant at Chebychev points, p_N , an accurate approximation of g for a sufficient number of interpolation points, in addition, the derivative of this polynomial, p'_N , is an accurate approximation of g' . Furthermore, Theorem 4.1..1 states that the rate of convergence of this approximation is exponential as the number of interpolation points increases. That is,

$$|g' - p'_N| = \mathcal{O}(K^{-N}). \quad (4.5)$$

Note that this K might be different from the K in (4.4). Since polynomial interpolation and polynomial differentiation are both linear operations, this leads to the development of a numerical differentiation method.

Chebyshev pseudo-spectral differentiation works in the following way:

Let $\{\xi_j\}_{j=1}^N$ be a Chebyshev grid of N points from 1 to -1 (4.1) and let $\{g(\xi_j)\}_{j=1}^N$ be the function values at these points.

1. Let $p_N(\xi)$ be the unique polynomial of degree at most $N - 1$ that interpolates g on the Chebyshev grid.
2. Then $w_N(\xi) = p'_N(\xi)$ is an approximation to g' from 1 to -1.

Given a vector of function values \vec{g}_N at Chebyshev points, this reduces to multiplication by a $N \times N$ matrix. That is, $\vec{w}_N = D_N \vec{g}_N$, where \vec{w}_N is a vector of the values of $w(\xi)$ at the Chebyshev points.

A MATLAB function that implements this, called `cheb.m` by Trefethen, is available at <http://www.comlab.ox.ac.uk/oucl/work/nick.trefethen> [5]. The function takes the degree of polynomial ($N - 1$) as input and outputs the $N \times N$ differentiation matrix as well as the Chebyshev grid with N points.

The notation used in this paper differs slightly from Trefethen [5] in that the indexing begins at 1 instead of 0. This is more convenient because MATLAB begins indexing at 1. Also, since this paper will be referring much more often to the number of interpolation points than to the degree of interpolating polynomial, it is also more convenient to make N the number of interpolation points.

4.3. Application to the ocean eigenvalue problem

In summary, given the assumption of the analyticity of the solution, and for sufficiently large N , a good approximation to the solution q of (3.3) is q_N , the vector of

polynomials interpolant at Chebychev points. Furthermore, to estimate $\frac{\partial \hat{v}_r}{\partial y}$ and $\frac{\partial}{\partial y} \Delta \hat{p}_r$, the corresponding parts of $q'_N(y)$ serve as good approximations. Using these approximations, (3.3) reduces to an algebraic eigenvalue problem involving a $6N \times 6N$ matrix with $N \times N$ blocks for each dependent variable $\hat{u}_r, \hat{v}_r, \Delta \hat{p}_r$, $r = 1, 2$.

5. DISCRETIZATION OF THE EIGENVALUE PROBLEM

Let $\xi_j = \cos((j-1)\pi/(N-1))$ for $j = 1, 2, \dots, N$ be a Chebychev grid on the interval $[-1, 1]$. Note that that $\xi_1 = 1$ and $\xi_N = -1$ so these points go from right to left. Then, let $L = 160000$, half the width of the channel, and let $y_j = -L\xi_j$. Thus, $\{y_j\}_{j=1}^N$ are the Chebychev interpolation points (4.1) scaled so that y_1 is at the South edge of the domain and y_N is the North edge. Let k and ω be fixed and consider q a function of y only, and for values of q at the Chebychev points write $q(y_j)$ for $j = 1, 2, \dots, N$. Let

$$U_r = [\hat{u}_r(y_1), \hat{u}_r(y_2), \dots, \hat{u}_r(y_N)]^T$$

$$V_r = [\hat{v}_r(y_1), \hat{v}_r(y_2), \dots, \hat{v}_r(y_N)]^T$$

$$P_r = [\Delta \hat{p}_r(y_1), \Delta \hat{p}_r(y_2), \dots, \Delta \hat{p}_r(y_N)]^T$$

and let

$$q_N = \begin{bmatrix} U_1 \\ V_1 \\ P_1 \\ U_2 \\ V_2 \\ P_2 \end{bmatrix}.$$

This is a column vector of the function values at the interpolation points. It has length $6N$. Now let

$$F = \begin{bmatrix} f(y_1) & 0 & \cdots & 0 \\ 0 & f(y_2) & \cdots & 0 \\ \vdots & \vdots & \ddots & \vdots \\ 0 & 0 & \cdots & f(y_N) \end{bmatrix}$$

be the $N \times N$ matrix with the discretized Coriolis parameter at the Chebychev points on the diagonal using the β -plane approximation $f(y) = f_0 + \beta y$. (See Section 3.1.) Also, replace each derivative with a Chebychev differentiation matrix $D_{y,N}$ with appropriate scaling. Also let $K_r = ik\alpha_r I_N$ and let $Q_r = ik\Delta\tilde{p}_r I_N$ where I_N is the $N \times N$ identity matrix. So, the differential-algebraic eigenvalue problem (3.3) becomes the purely algebraic eigenvalue problem

$$(-i\omega)q_N = Gq_N \tag{5.1}$$

where

$$G = \begin{bmatrix} O & F & -K_1 & O & O & -K_2 \\ -F & O & -\alpha_1 D_{y,N} & O & O & -\alpha_2 D_{y,N} \\ -Q_1 & -\Delta\tilde{p}_1 D_{y,N} & O & O & O & O \\ O & O & -K_2 & O & F & -K_2 \\ O & O & -\alpha_2 D_{y,N} & -F & O & -\alpha_2 D_{y,N} \\ O & O & O & -Q_2 & -\Delta\tilde{p}_2 D_{y,N} & O \end{bmatrix}. \tag{5.2}$$

Here O is the $N \times N$ zeros matrix.

Now consider the matrix operator $D_{y,N}$. The Chebychev grid that `cheb.m` outputs is between 1 and -1, so it must be scaled to the width of the channel. Also the order must be reversed so that the y values go from South to North in order. Similarly, a scaling factor is needed with the differentiation matrix from the chain rule.

Now, if $y_j = -L\xi_j$ for $j = 1, 2, \dots, N$, then $q(y_j) = q(-L\xi_j) = g(\xi_j)$. So, $q'(y) = g'(\xi) \frac{d\xi}{dy} = g'(\xi)(-L^{-1})$. Thus if D_N is the $N \times N$ Chebychev differentiation matrix on the interval from -1 to 1, $q'(y) \approx -L^{-1}D_N g_N(\xi) = -L^{-1}D_N q_N(y)$. Thus, the desired differentiation matrix is $D_{y,N} = -L^{-1}D_N$.

So, G can be rewritten, replacing $D_{y,N}$ with $-L^{-1}D_N$, as

$$G = \begin{bmatrix} O & F & -K_1 & O & O & -K_2 \\ -F & O & \alpha_1 L^{-1} D_N & O & O & \alpha_2 L^{-1} D_N \\ -Q_1 & \Delta \tilde{p}_1 L^{-1} D_N & O & O & O & O \\ O & O & -K_2 & O & F & -K_2 \\ O & O & \alpha_2 L^{-1} D_N & -F & O & \alpha_2 L^{-1} D_N \\ O & O & O & -Q_2 & \Delta \tilde{p}_2 L^{-1} D_N & O \end{bmatrix}. \quad (5.3)$$

5.1. Boundary conditions

From Section 3., the boundary conditions are

$$v_r(y_S) = v_r(y_N) = 0 \quad \text{for } r = 1, 2.$$

Now, since the South and North walls are at y_1 and y_N respectively, in the discretized eigenvalue problem the boundary condition is

$$\hat{v}_r(y_1) = \hat{v}_r(y_N) = 0 \quad \text{for } r = 1, 2.$$

This boundary condition requires that these four entries of q_N are zero. Specifically they are the $N + 1$, $2N$, $4N + 1$, and $5N$ th entries. For an eigenvalue problem, if an entry of an eigenvector is known to be zero, the column of the multiplying matrix corresponding to that entry might as well be zero as it is always multiplied by zero. That is, if $c_i = [c_{1,i} \ c_{2,i} \ \cdots \ c_{N,i}]^T$ is the i th column of the multiplying matrix, and v the eigenvector with eigenvalue λ , then $\lambda v_j = c_{j,i}v_i + \sum_{k \neq i} c_{j,k}v_k$, where v_j is the j th entry of v . Since $v_i = 0$ is known, $\lambda v_j = \sum_{k \neq i} c_{j,k}v_k$ and no information is lost by setting $c_{j,i} = 0$. Thus the columns $N + 1$, $2N$, $4N + 1$ and $5N$ of G can be set to zero.

Now, consider a row of the multiplying matrix corresponding to a zero entry of an eigenvector. This row only determines that entry and does not affect any other entry. That is, if $r_i = [r_{i,1} \ r_{i,2} \ \cdots \ r_{i,N}]$ is a row of the multiplying matrix, and v an eigenvector with eigenvalue λ , then

$$r_i v = \lambda v_i.$$

In particular, if v_i is known to equal zero,

$$r_i v = 0.$$

Thus r_i can also be replaced with zeros for $i = \{N + 1, 2N, 4N + 1, 5N\}$ without losing any information, and this guarantees that the boundary conditions are satisfied.

However, this method will clearly give 0 as an eigenvalue with multiplicity at least four. This can be avoided by deleting the mentioned rows and columns. Care must be taken in coding this correctly in MATLAB, deleting rows from bottom to top and columns from right to left to avoid indexing errors.

5.2. Eigenvalues and eigenvectors

As stated above, the goal is to solve the eigenvalue problem $(-i\omega)q = Gq$. So, use the `eig` function in MATLAB to compute the eigenvalues and eigenvectors of G . The

eigenvalues are $\lambda = -i\omega$, so the frequency ω can be recovered as the imaginary part of an eigenvalue λ . The eigenvectors correspond to the cross-channel spatial dependence of modal solutions. The first N entries correspond to \hat{u}_1 . The next $N - 2$ entries correspond to \hat{v}_1 , as q does not include the values of \hat{v} at the boundary where it is zero. The next N entries correspond to $\Delta\hat{p}_1$. The next $3N - 2$ entries correspond to the same information, but for the second layer.

Finally, to recover the solutions u_r , v_r and Δp_r at any x and t , multiply the eigenvectors by $e^{ikx - i\omega t}$ to reverse the substitution in (3.2) and use the real part of the result.

6. RESULTS

This section explores the results of the scheme described in Section 5. and shows that these results are consistent with the theory discussed in Section 2.. Mainly, this section will explore the Rossby waves produced by this scheme, demonstrating their existence as well as examining dispersion relations and a few internal and external modes. Additionally, this section will briefly discuss the Kelvin waves.

6.1. Existence of Rossby modes using this scheme

Figure 6.1 shows a plot of the absolute values of the eigenvalues of G with $N = 32$, so that there are $6 \times 32 - 4 = 188$ modes. A question that arises is the following: Which, if any, of these eigenvalues correspond to Rossby modes? Note that there appear to be three main “clusters”. It turns out that the first of these is made up of Rossby modes while the second two clusters are made up of gravity modes. To see this, instead of building the

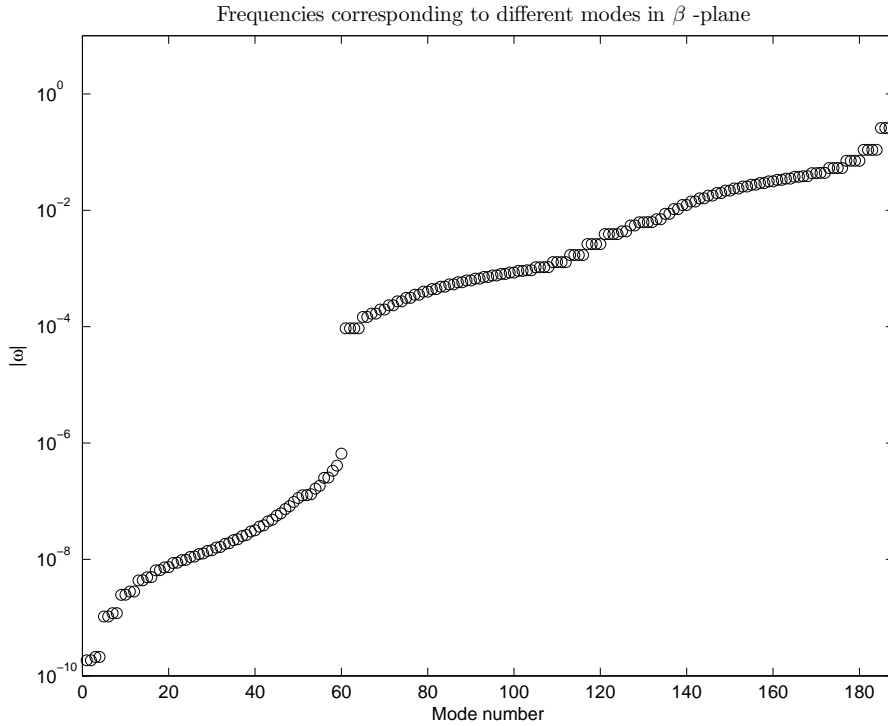


FIGURE 6.1: Eigenvalues with variable Coriolis parameter. Here the Coriolis parameter is given by $f(y) = f_0 + \beta y$ where f_0 is the Coriolis parameter at 45° N, the center of the channel. The eigenvalues are ordered according to absolute value and the mode number just refers to this ordering. The number of interpolation points in this case is $N = 32$, so there are $6 * N - 4 = 188$ modes. Modes from 1-60 are Rossby modes with external and internal modes generally alternating. Closer to 60 are the well-resolved modes. Modes 61-123 are internal gravity modes. Of these, modes 61-64 are the internal Kelvin modes, immediately followed by the internal Poincaré modes. Modes 124-188 are external gravity modes. Modes 124-127 are Kelvin modes and are immediately followed by the external Poincaré modes.

matrix block F as in Section 5., set $f(y) = f_0$ for all y . By removing the dependence of f on y , this changes the problem from being a β -plane problem to an f -plane problem. Upon plotting the eigenvalues again, the first cluster drops to about machine epsilon (Figure 6.2). Thus, the first cluster only exists if the Coriolis parameter varies over y . Hence, these are Rossby modes and the remaining modes are gravity modes. Furthermore, these modes have qualities consistent with their identification as Rossby modes, as demonstrated next.

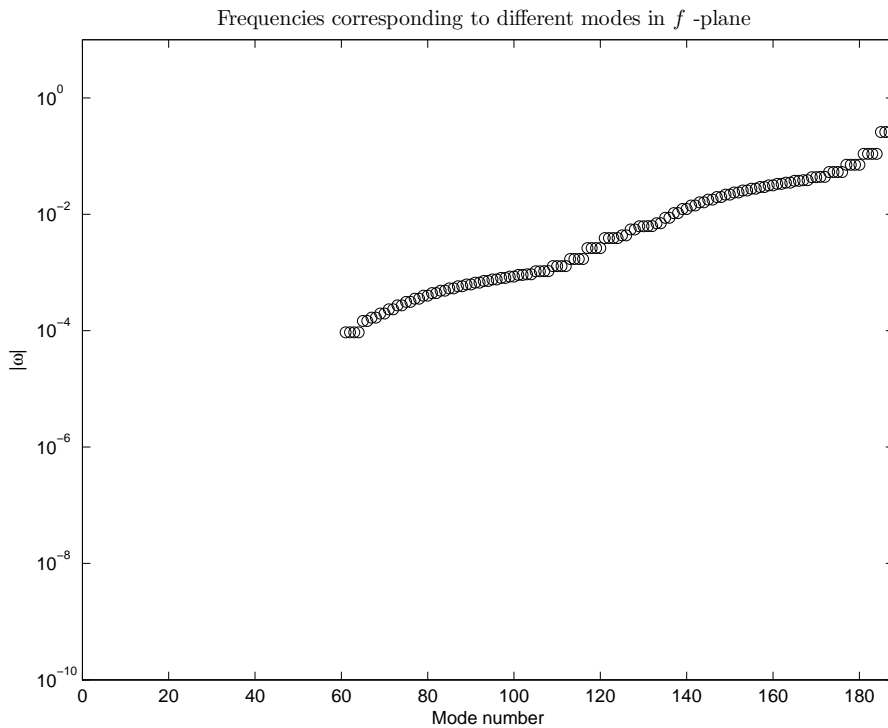


FIGURE 6.2: Eigenvalues with fixed Coriolis parameter. Here the Coriolis parameter is given by $f = f_0$ where f_0 is the Coriolis parameter at the 45° N, the center of the channel. Here modes 61-188 appear as they did in Figure 6.1, but modes 1-60 do not appear. They are not shown because they are very near machine epsilon. This demonstrates that these modes only exist because of the dependence of f on y in the β -plane problem.

6.2. Dispersion relation for Rossby waves

Figure 6.3 shows the dispersion relation for some of the Rossby modes demonstrated to exist in Section 6.1. That is, it shows the dependence of ω on k for a given mode. Both internal and external modes are shown.

The shape and scale of these dispersion relations match those found by Higdon using finite differences [2]. Figure 6.3 shows that, since $\omega < 0$ everywhere, for any particular mode the phase velocity $\omega/k < 0$. Thus, the individual mode propagates in the negative, or westward, direction. However, the group velocity, $d\omega/dk$ is negative for very small k (long wavelength) and positive for larger k (short wavelength). Thus wave packets of very short Rossby waves propagate eastward, but wave packets of longer Rossby waves

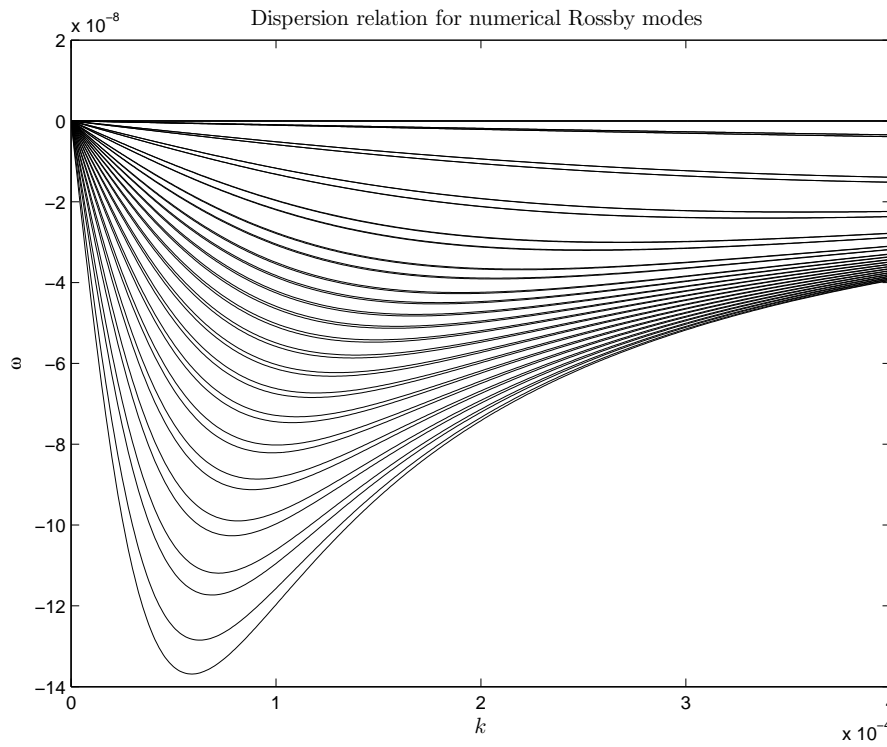


FIGURE 6.3: Dispersion relations for some numerical Rossby modes. Here $\Delta x = 10$ km. Observe that for all values of k , the phase velocity w/k is negative (westward). However, while for small values of k (long wavelengths) the group velocity $d\omega/dk$ is negative (westward), the group velocity for larger values of k (short waves) is have positive (eastward).

propagate westward. This happens for k greater than approximately 10^{-4} . Thus, in this channel, long Rossby waves have wavelengths greater than about 60 km in the x direction. All of the Rossby modes examined in the following section are of the long, westward-propagating type. This scale is consistent with experimental data. For example, Gill cites the observation of Rossby waves with periods of 4-11 months and wavelengths of 170-300 km [1].

6.3. Contour plots and velocity fields

Figures 6.4-6.11 are contour plots of the first few Rossby modes at $t = 0$, external and internal, together with their velocity fields. Observe that the external modes have

the same profile in both layers, proportional to layer thicknesses. Note also that the internal modes have opposite profiles so that the total free-surface perturbation is nearly zero. Furthermore, observe that the arrows indicating the velocity field are tangent to level curves. This shows that the waves are in near geostrophic balance, consistent with physical Rossby waves. Thus, qualitatively these solutions have the characteristics expected of Rossby waves.

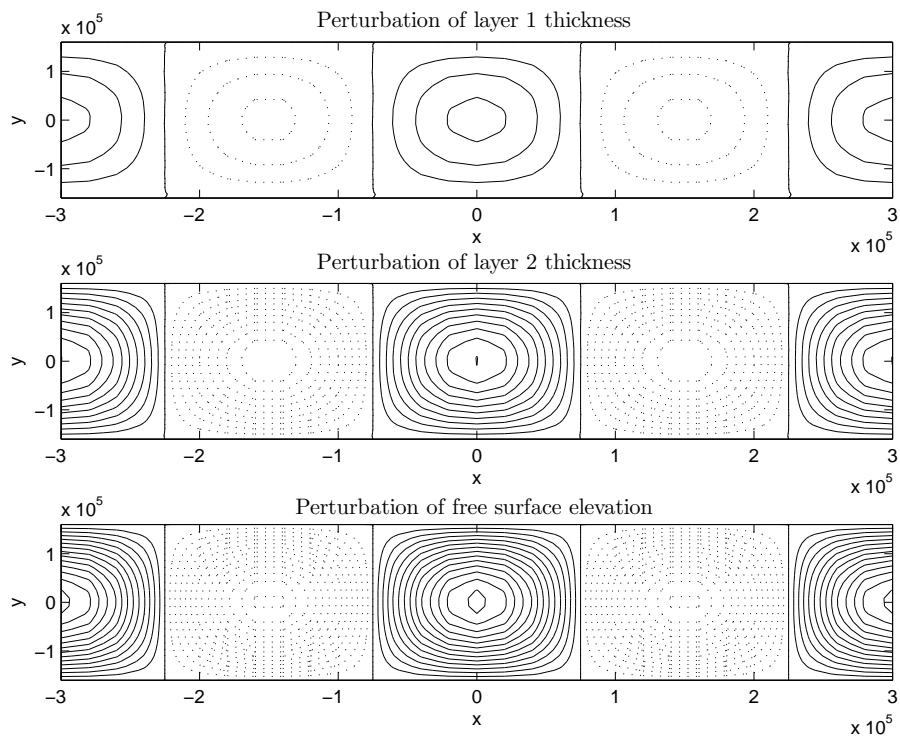


FIGURE 6.4: First external Rossby mode. This shows the perturbation of the layer thickness for layers 1 and 2 as well as the perturbation in the free-surface elevation. Solid curves correspond to positive perturbation and dotted lines to negative perturbation. This mode corresponds to mode number 60 in Figure 6.1 and is the first external Rossby mode in the sense that it is the external Rossby mode that varies least in the cross-channel direction. In each subplot the intervals between contours are the same. Since there are three times more contours in the plot of layer 2, the perturbation in the thickness of layer 2 is three times greater than the perturbation in the thickness of layer 1. This is consistent since layer 2 is three times thicker than layer 1 at equilibrium. Notice that the layers thicken or thin together, so that the effect on the free-surface elevation is the sum of the perturbations in each layer. Thus there are four times as many contours in the plot showing perturbation in free-surface elevation as there are in the plot showing perturbation in the thickness of layer 1.

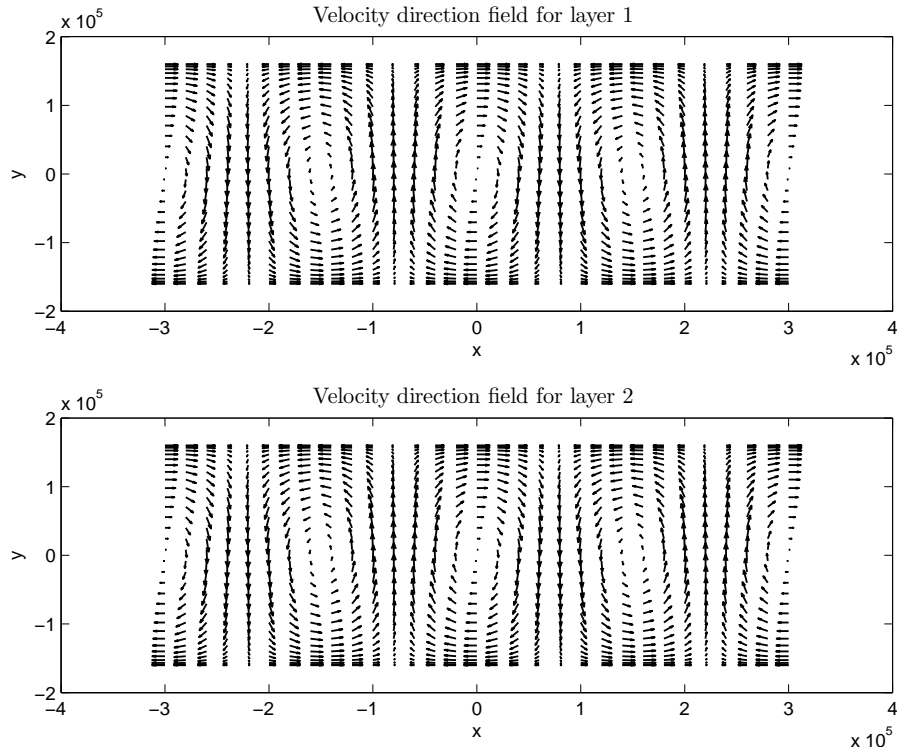


FIGURE 6.5: Velocity fields for the first external Rossby mode. These are the velocity fields corresponding to the mode shown in Figure 6.4. Observe that the velocity field arrows are approximately tangent to the level curves shown in Figure 6.4 with clockwise circulation corresponding to crests and counterclockwise circulation corresponding to troughs. Also, at any point the circulation is in the same direction in both layers. This is characteristic of external Rossby modes.

6.4. Kelvin modes

This scheme outputs four Kelvin waves, two along the North edge of the channel, one internal and one external, and two along the South edge of the channel, one internal and one external. The waves propagating along the North edge of the channel have negative phase speeds, so they are travelling westward, while the waves propagating along the South edge of the channel have positive phase speeds, so they are traveling eastward. Thus these waves are travelling in a counterclockwise fashion. Since the channel is in the northern hemisphere, this is consistent with the theory described in Section 2.. For each Kelvin wave, this scheme outputs an eigenspace of dimension two. MATLAB outputs

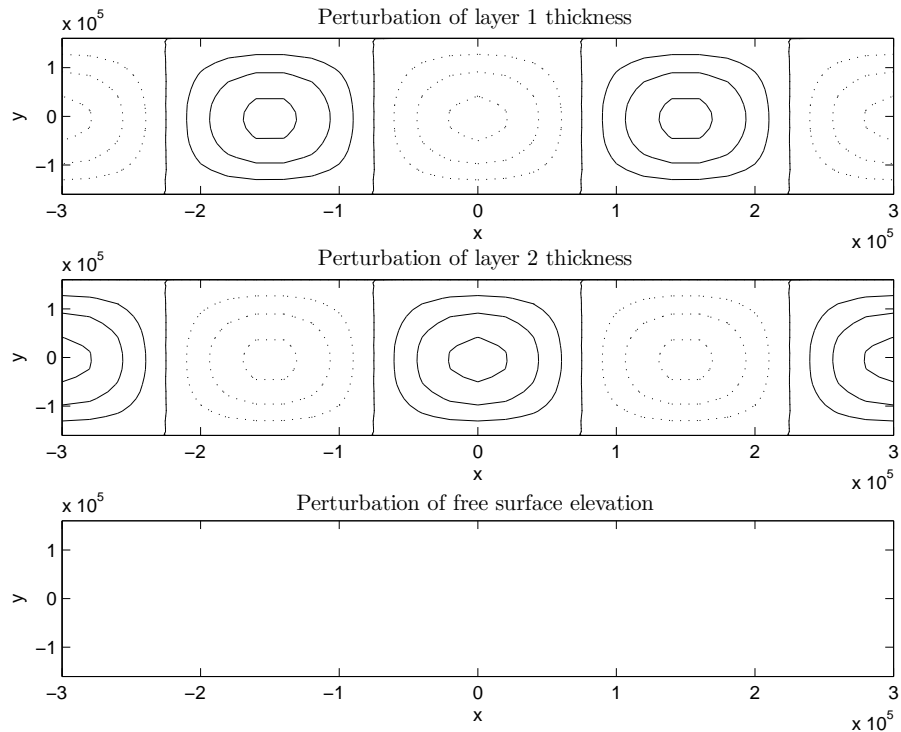


FIGURE 6.6: First internal Rossby mode. This mode corresponds to the mode number 58 from Figure 6.1. Again, “first” refers to the fact that this is the internal Rossby mode with the least variation in the cross-channel direction. Here the number of contours is the same in both layers but where layer 1 has a positive perturbation, layer 2 has a negative perturbation and vice versa. Thus the net effect on the free-surface perturbation is nearly zero. Thus the plot showing free-surface elevation is blank.

two eigenvectors forming a basis for this eigenspace. These eigenvectors have unphysical oscillations, but linear combinations of these eigenvectors lead to the non-oscillatory, smooth Kelvin waves. Figure 6.12 shows the cross-channel profile at $x = 0$ and $t = 0$ of the internal Kelvin wave that travels along the South edge of the channel. Observe the exponential decay from the South edge in Δp_r . The velocity component v is zero in this cross-section, because when $x = 0$, v is purely imaginary.

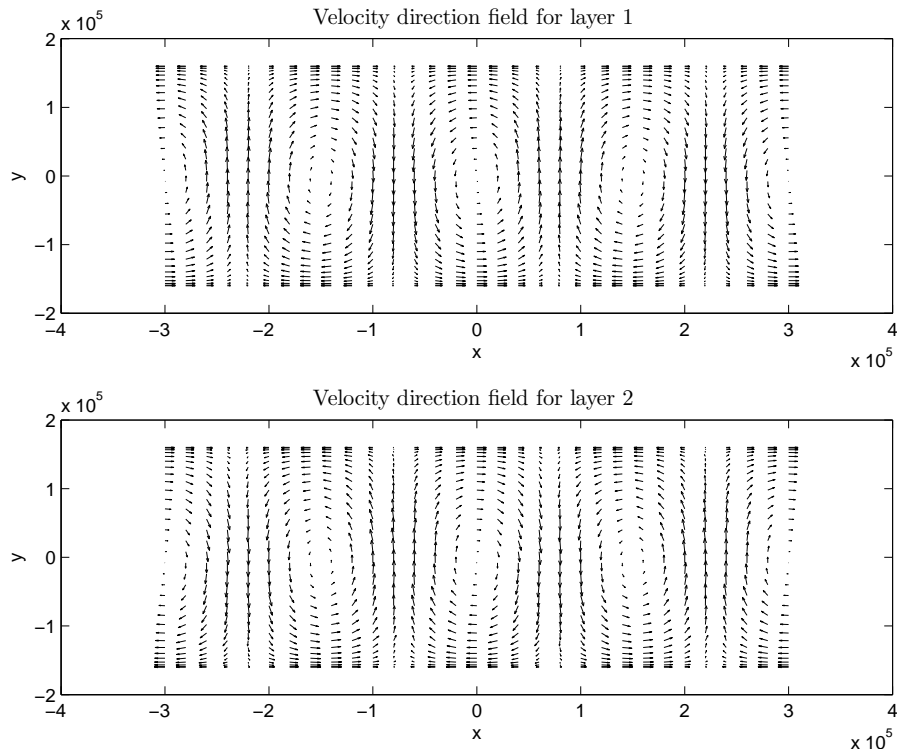


FIGURE 6.7: Velocity fields for the first internal Rossby mode. These are the velocity fields corresponding to layer 1 and layer 2 in the mode shown in Figure 6.6. Observe that the layers show circulation along the level curves as in the external mode, but that layers circulate in opposite directions. In fact, the mass-weighted average of the velocities in the two layers is nearly zero. In the thinner layer, layer 1, the magnitude of the velocity is 3 times that of layer 2. While it is true, this is difficult to see using this type of plot.

7. EXACT SOLUTIONS FOR A SPECIAL CASE

The goal of this section is to show convergence to an exact solution in a special case. When the thickness of one layer is much smaller than that of the other, or when both layers have the same density, the two-layer system degenerates into the Linearized Shallow-Water Equations (LSWE). There are special cases in which exact solutions of the LSWE are known. One example of this is found in Paldor et al. [4]. Here, an analytic solution is derived for the single layer LSWE on an f -plane that may not be physical, but serves to check the solutions produced by the above method.

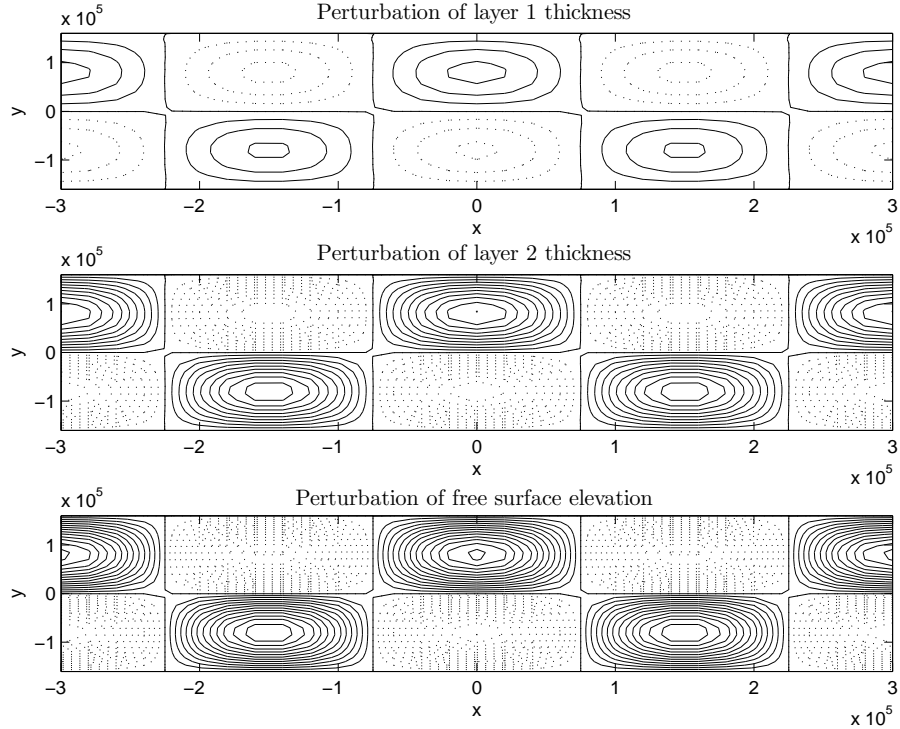


FIGURE 6.8: Second external Rossby mode. This mode corresponds to mode number 59 in Figure 6.1.

Once again, consider a channel of shallow water 320 km wide in the y direction, with total depth 4000 m. The single layer LSWE can be stated

$$\begin{aligned}
 \frac{\partial u}{\partial t} - f(y)v &= -g \frac{\partial \eta}{\partial x}, \\
 \frac{\partial v}{\partial t} + f(y)v &= -g \frac{\partial \eta}{\partial y}, \\
 \frac{\partial \eta}{\partial t} &= -H \left(\frac{\partial u}{\partial x} + \frac{\partial v}{\partial y} \right),
 \end{aligned} \tag{7.1}$$

where η is the perturbation in surface elevation and H is the equilibrium thickness of the fluid. $f(y)$ is the Coriolis parameter as above, which can be written $f_0 + \beta y = 2\Omega(\sin(\phi_0) + \cos(\phi_0)y/R)$. Here ϕ_0 is the latitude of the center of the channel, Ω is the earth's rotation frequency and R is the earth's radius. Paldor [4] changes variables to get a nondimensionalized version of (7.1),

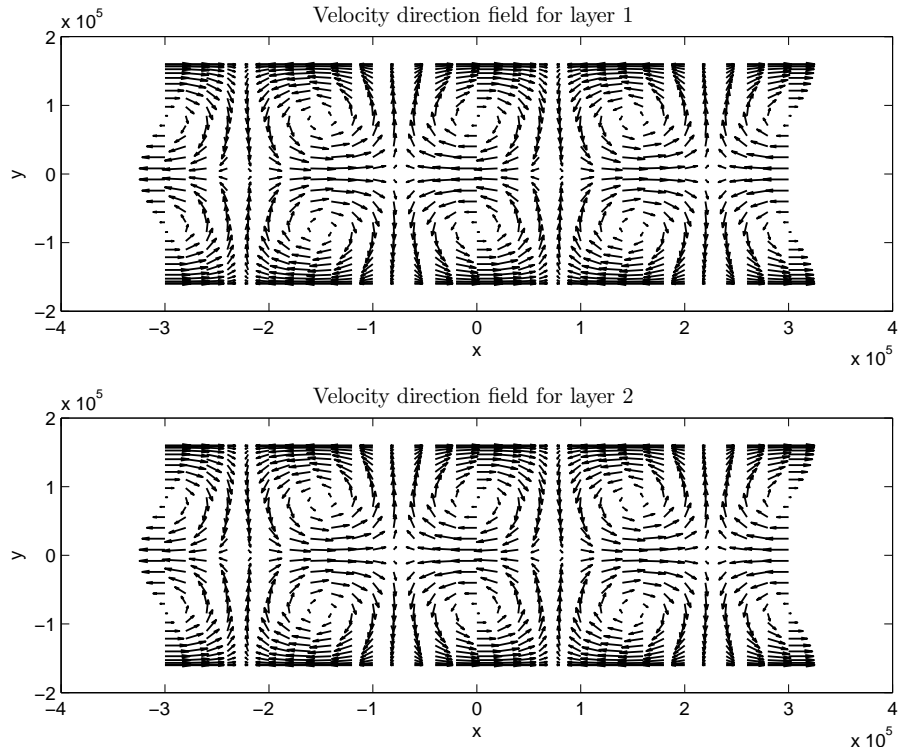


FIGURE 6.9: Velocity fields for the second external Rossby mode. These velocity fields correspond to the mode shown in Figure 6.8.

$$\begin{aligned}
 \frac{\partial u}{\partial t} - (\sin(\phi_0) + \cos(\phi_0)y)v &= -\alpha \frac{\partial \eta}{\partial x} \\
 \frac{\partial v}{\partial t} + (\sin(\phi_0) + \cos(\phi_0)y)u &= -\alpha \frac{\partial \eta}{\partial y} \\
 \frac{\partial \eta}{\partial t} &= -\left(\frac{\partial u}{\partial x} + \frac{\partial v}{\partial y}\right),
 \end{aligned} \tag{7.2}$$

where $\alpha = gH/(2\Omega R)^2$.

Assume that the solution is of the form

$$\begin{aligned}
 (u(x, y, t), v(x, y, t), \eta(x, y, t))^T &= q(x, y, t) \\
 &= \hat{q}(k, y, \omega)e^{ikx - i\omega t} \\
 &= \hat{q}(k, y, \omega)e^{ik(x - Ct)}.
 \end{aligned}$$

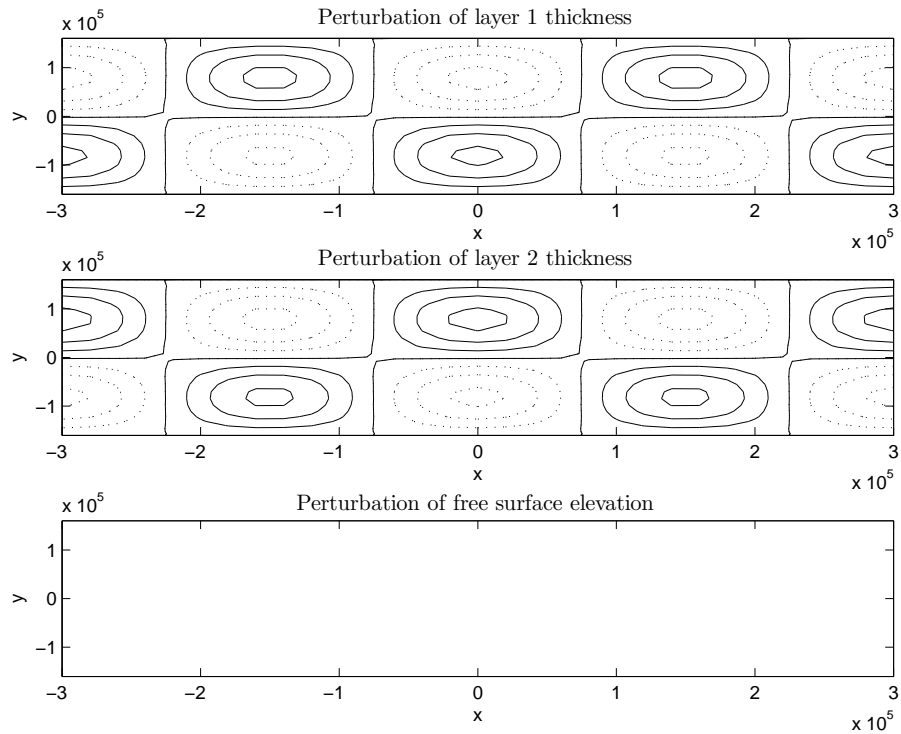


FIGURE 6.10: Second internal Rossby mode. This mode corresponds to the mode number 57 in Figure 6.1.

The last line leads to the substitution

$$u = \hat{u}e^{ik(x-Ct)}$$

$$v = \hat{v}e^{ik(x-Ct)}$$

$$\eta = \hat{\eta}e^{ik(x-Ct)}.$$

Paldor [4] also uses the substitution $V(y) = iv(y)/k$. After some algebra, the system (7.2) becomes

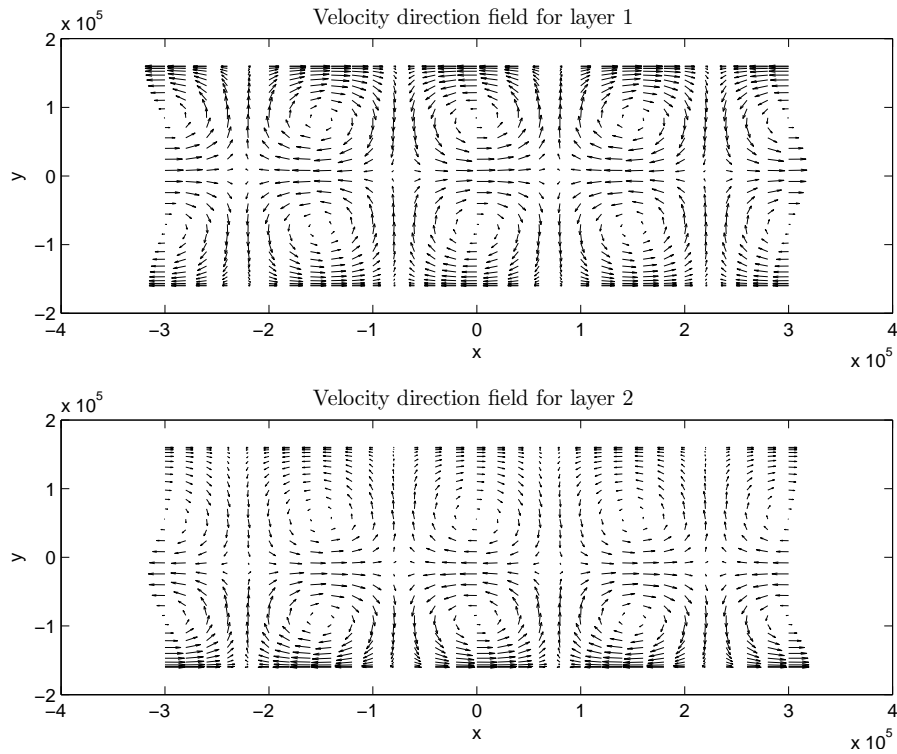


FIGURE 6.11: Velocity fields for the second internal Rossby mode. These velocity fields correspond to the mode shown in Figure 6.10.

$$u = \frac{\sin(\phi_0) + \cos(\phi_0)y}{C}V + \frac{\alpha}{C}\eta \quad (7.3)$$

$$\frac{dV}{dy} = \frac{\sin(\phi_0) + \cos(\phi_0)y}{C}V + \left(\frac{\alpha}{C} - C\right)\eta \quad (7.4)$$

$$\frac{d\eta}{dy} = \frac{k^2C^2 - [\sin(\phi_0) + \cos(\phi_0)y]^2}{\alpha C}V - \frac{\sin(\phi_0) + \cos(\phi_0)y}{C}\eta \quad (7.5)$$

The first line, (7.3), is an algebraic expression for u in terms of V and η . (7.4)-(7.5) do not involve u , so to solve the whole system, it is only necessary to solve the system comprised of the last two lines. Now, differentiating (7.4), and using (7.4) and (7.5) to eliminate η , the result is a single Schrödinger equation in V that can be written in terms of $z \in [-1, 1]$,

$$\epsilon^2 \frac{d^2V}{dz^2} + [E - (1 + bz)^2]V = 0, \quad (7.6)$$

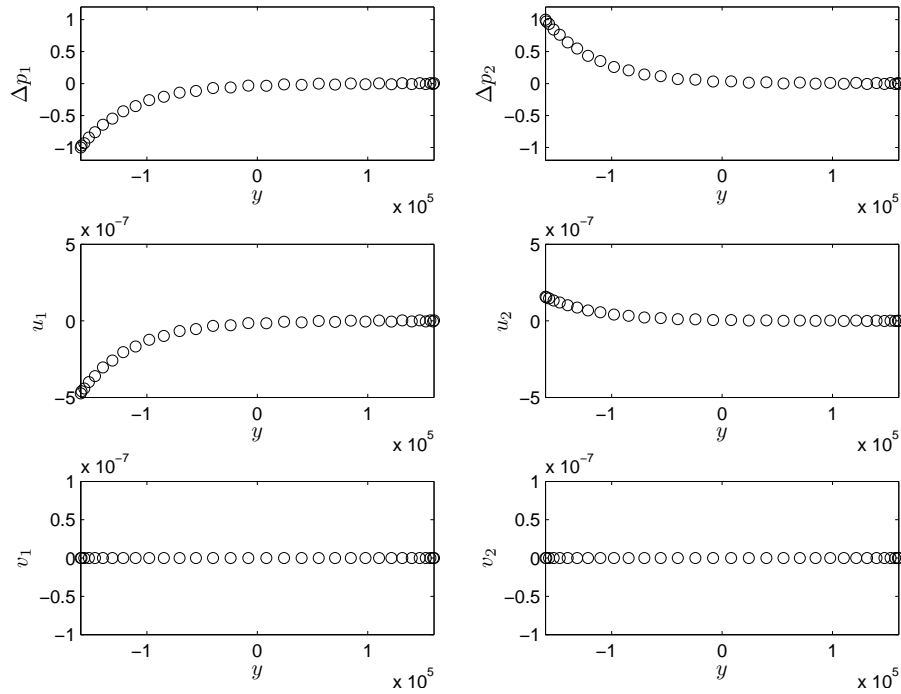


FIGURE 6.12: A Kelvin mode. This is the cross-channel profile of the internal Kelvin wave that travels along the South edge of the channel. The first column of figures corresponds to the upper layer, and the second column corresponds to the lower layer. Note that, consistent with the theory, there is exponential decay in Δp_r from one side of the domain. Furthermore, the phase velocity of this wave is found to be positive, thus this wave is travelling eastward. This is also consistent with the theory that states that Kelvin waves propagate in a counterclockwise fashion in the northern hemisphere.

with the boundary conditions $V(-1) = V(1) = 0$. Here,

$$\epsilon = \frac{\sqrt{\alpha}}{\sin(\phi_0)L}$$

$$b = \frac{\cos(\phi_0)L}{\sin(\phi_0)}$$

$$E = -\frac{\alpha}{\sin^2(\phi_0)} \left[\frac{\cos(\phi_0)}{C} + k^2 \left(1 - \frac{C^2}{\alpha} \right) \right].$$

Paldor [4] shows that for the case $b = 0$ this has eigensolutions

$$V_n(z) = \frac{2}{\pi(n+1)} \sin \left[\frac{(n+1)\pi}{2}(z+1) \right]$$

with corresponding eigenvalues

$$E_n = 1 + \left[\frac{\pi\epsilon(n+1)}{2} \right]^2$$

for $n = 0, 1, 2, \dots$

The condition $b = 0$ means that $\cos(\phi_0) = 0$, thus $\phi_0 = \pi/2$, that is, the North pole is the center of the channel. As stated before, this is not physically meaningful; however, mathematically it is meaningful, and it gives a way to check the results of the Chebychev pseudo-spectral method presented in this paper. The parameter $b = 0$ also means that $\beta = 0$. Thus, this is the f -plane case and so only gravity waves will be present as solutions, not Rossby waves.

7.1. Convergence of Chebychev solution to analytic solution

Returning to the two-layer system, let the densities of the two layers be equal and let $\beta = 0$, with the center of the channel at $\phi_0 = \pi/2$. Since the layers have equal densities, the system only includes external waves. Take the perturbation in free-surface elevation to be the sum of the layer thickness perturbations and compare this with the analytic solution of the one-layer case.

Figures 7.1 and 7.3 compare the first two modes in each system after normalization. The results of the Chebychev approximation are very nearly exact. Let V_n be the n th mode of the exact solution at the Chebychev points and V_N^n be the i/k times the cross-channel velocity part of the corresponding mode of the Chebychev approximation. N refers the number of interpolation points used. Consider the maximum error at the Chebychev points, given by

$$\mathcal{E}_N^n = \max(|V_n - V_N^n|).$$

Figures 7.2 and 7.4 show $\log_{10}(\mathcal{E}_N^n)$ plotted against the number of interpolation points N . Note that at about 20 interpolation points this method leads to very high accuracy. The nearly linear relation shown implies the exponential rate of convergence,

$$\mathcal{E}_N^n = \max |V_n(y) - V_N^n(y)| = \mathcal{O}(K^{-N}). \quad (7.7)$$

This is the rate of convergence expected from Theorem 1 given that the solution is analytic on a certain region. According to Paldor [4], the exact solutions of (7.6) are parabolic cylinder functions, which are entire. Thus, they satisfy the hypothesis of Theorem 4.1.1 and exponential convergence is expected.

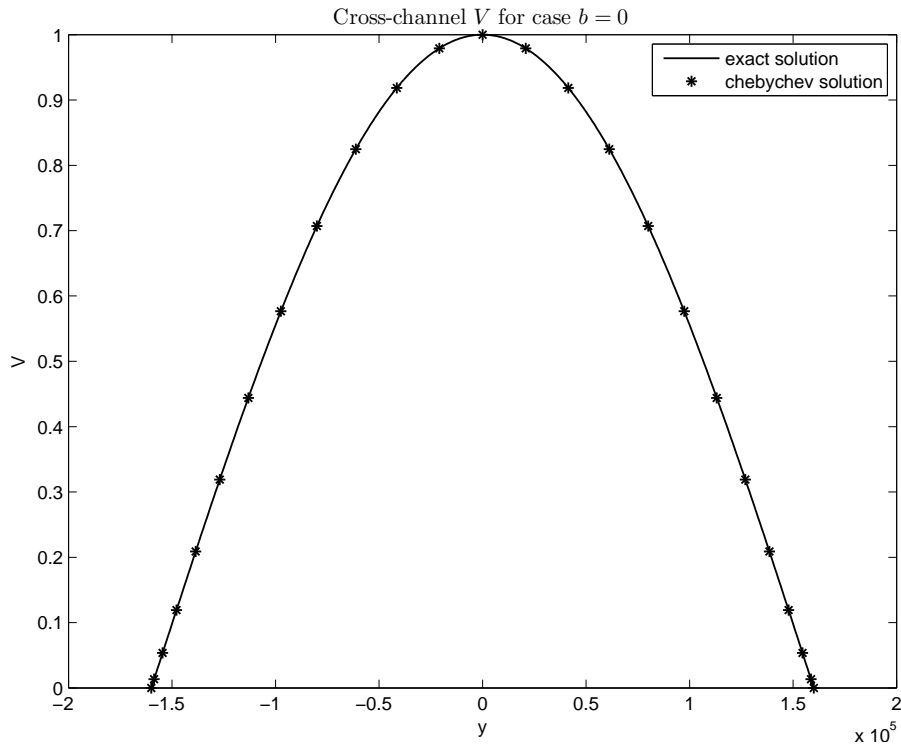


FIGURE 7.1: Normalized cross-channel velocity, exact and approximate, for the first Poincaré mode. V is an imaginary constant multiple of the cross-channel velocity. This plot shows the cross-channel profile of V for $x = 0$. Here both solutions are normalized to have maximum value 1.

8. CONCLUSION

The goal of this paper is to present near analytic solutions for a numerical ocean circulation test problem. The test problem developed in this paper is for a two-layer

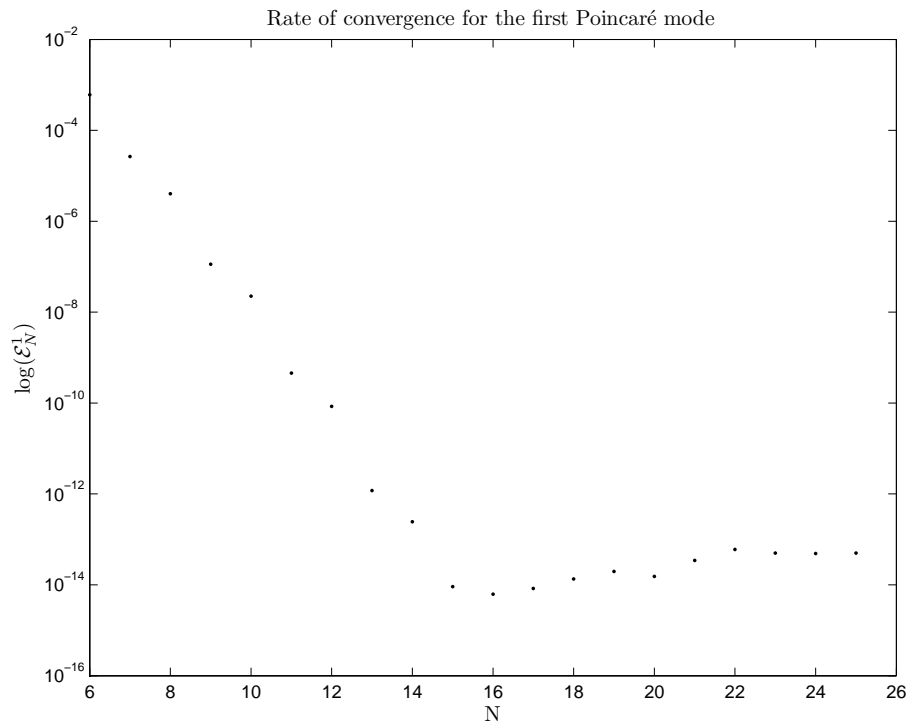


FIGURE 7.2: The rate of convergence of the max-norm error. The error here is taken to be the maximum difference between the approximated solution and the exact solution at interpolation points. The vertical axis shows the base 10 logarithm of this error. There is a slight difference in error between the even and odd number of interpolation points. Still, the relation between the number of interpolation points and the logarithm of the max-error is nearly linear. Thus, the error decreases exponentially as the number of interpolation points increase. This is consistent with the order of convergence given in Theorem 4.1.1.

fluid in an East-West channel. A β -plane approximation of the variation of the Coriolis parameter across the channel is used, so this system includes both Rossby and gravity waves. First, the system is transformed into a differential-algebraic eigenvalue problem. Then, to compute the solutions of this eigenvalue problem to a high degree of accuracy, a pseudo-spectral method is used. This method is based on the concept of first interpolating a function on a non-uniform, Chebychev grid and then differentiating the interpolating polynomial and using this as an approximation to the derivative of the original function. Since interpolation and polynomial differentiation are both linear operations, this can be represented using matrix multiplication. The system is discretized in the cross-channel direction and then the derivatives are replaced with the Chebychev differentiation matrices.

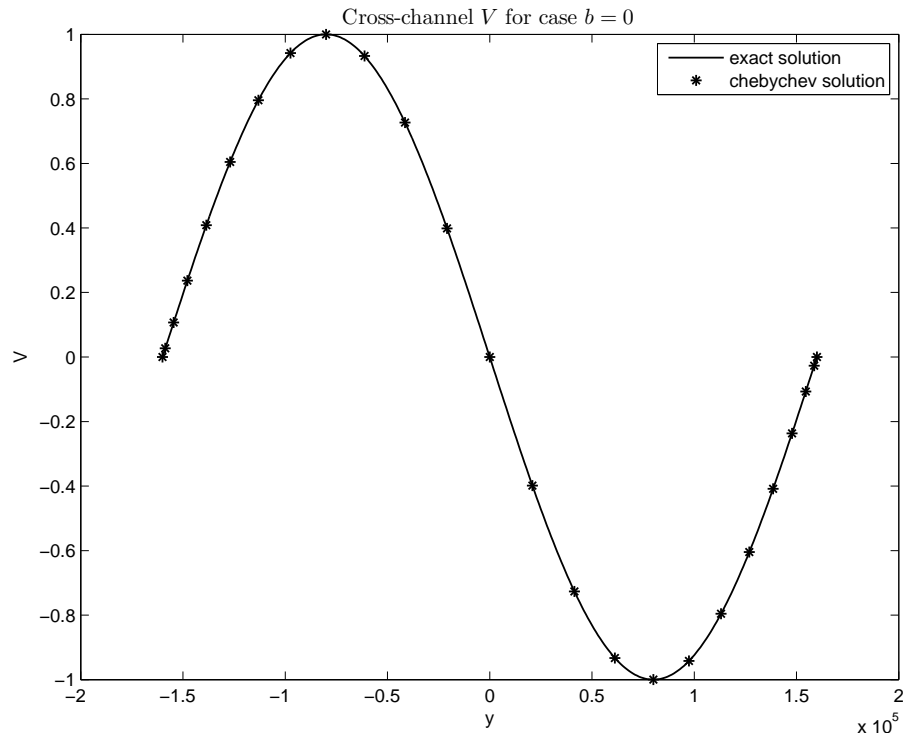


FIGURE 7.3: Normalized cross-channel velocity of the approximate and exact solutions for the second Poincaré mode.

These matrices are modified to impose hard-wall boundary conditions. The now purely algebraic eigenvalue problem is then solved.

To show that these solutions are indeed accurate, first it was shown that the numerically computed waves have the qualities that the physical waves are known to possess. Second, in the special case where the two-layer system degenerates to a one-layer system, some analytic solutions are known. In this case, it was shown that the numerical solutions converge with spectral accuracy to the analytic solutions.

In conclusion, it is reasonable to assume that the solutions produced here are very near exact and could be used as a test problem in numerical ocean circulation modeling.

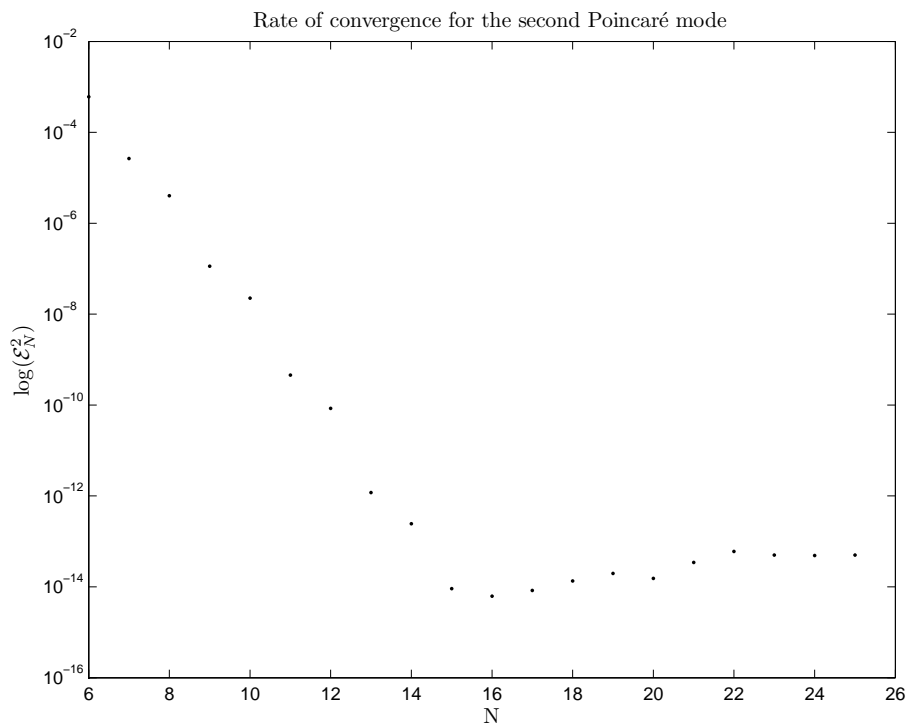


FIGURE 7.4: The rate of convergence of the max-norm error. A few more interpolation points are needed to reach the minimum error, but the rate of convergence is still clearly exponential. At about 20 interpolation points the pseudo-spectral method produces a nearly exact solution.

BIBLIOGRAPHY

1. A.E. Gill, (1982) *Atmosphere-ocean dynamics*, Academic Press, New York.
2. R.L. Higdon, (2005) A two-level time-stepping method for layered ocean circulation models: further development and testing, *Journal of Computational Physics*, 206(2).
3. R.L. Higdon, (2006) Numerical modelling of ocean circulation, *Acta Numerica*, 15.
4. N. Paldor, S. Rubin, and A.J. Mariano, (2007) A consistent theory for linear waves of the shallow-water equations on a rotating plane in midlatitudes, *Journal of Physical Oceanography*, 37.
5. L.N. Trefethen, (2000) *Spectral Methods in Matlab: Software, Environments, Tools*, Society for Industrial and Applied Mathematics.

